Phase diagram for antiferromagnetism and superconductivity in the pressure-induced heavy-fermion superconductor Ce_2RhIn_8 probed by ^{115}In-NQR

M. Yashima,[1,2] S. Taniguchi,[1] H. Miyazaki,[1] H. Mukuda,[1,2] Y. Kitaoka,[1] H. Shishido,[3,*] R. Settai,[3] and Y. Ōnuki[3,4]
[1]*Department of Materials Engineering Science, Osaka University, Osaka 560-8531, Japan*
[2]*JST, Transformative Research-Project on Iron Pnictides (TRiP), Chiyoda, Tokyo 102-0075, Japan*
[3]*Department of Physics, Graduate School of Science, Osaka University, Osaka 560-0043, Japan*
[4]*Advanced Science Research Center, Japan Atomic Energy Research Institute, Tokai, Ibaraki 319-1195, Japan*
(Received 9 October 2009; published 9 November 2009)

We present a phase diagram for the antiferromagnetism and superconductivity in Ce_2RhIn_8 probed by In-NQR studies under pressure (P). The quasi-two-dimensional character of antiferromagnetic spin fluctuations in the paramagnetic state at $P=0$ evolves into a three-dimensional character because of the suppression of antiferromagnetic order for $P>P_{QCP}\sim 1.36$ GPa (QCP: quantum critical point). Nuclear-spin-lattice relaxation rate $1/T_1$ measurements revealed that the superconducting order occurs in the P range 1.36–1.84 GPa, with maximum $T_c\sim 0.9$ K around $P_{QCP}\sim 1.36$ GPa.

DOI: 10.1103/PhysRevB.80.184503 PACS number(s): 74.25.Ha, 74.62.Fj, 74.70.Tx, 75.30.Kz

I. INTRODUCTION

The heavy-fermion (HF) compounds $CeIn_3$ (Refs. 1 and 2) and $CeTIn_5$ (T=Co, Rh, Ir) (Refs. 3–6) revealed an intimate relationship between antiferromagnetism (AFM) and superconductivity (SC).[7] $CeIn_3$ has a cubic crystal structure, and it is expected to exhibit the three-dimensional (3D) magnetic interaction. $CeIn_3$ is an antiferromagnet with $T_N=10$ K at ambient pressure ($P=0$), and AFM discontinuously collapses around $P_c=2.46$ GPa, suggesting that the quantum phase transition from AFM to paramagnetism (PM) is of the first order.[8,9] SC appears in a narrow pressure range $P=2.28-2.65$ around P_c, and T_c reaches the maximum value (~ 0.25 K) at P_c. Non-Fermi-liquid behaviors observed at pressures below P_c evolve into Fermi-liquid behaviors at pressures that just exceed P_c. It was suggested that the first-order quantum phase transition is responsible for the occurrence of SC in $CeIn_3$.[9]

$CeRhIn_5$, which has a tetragonal crystal structure, is also an antiferromagnet with $T_N=3.8$ K at $P=0$.[4] For $CeRhIn_5$, we have shown that the tetracritical point, where the AFM, AFM+SC, SC, and PM phases are in contact, exists at $P_{tetra}\sim 1.98$ GPa and T_c reaches the maximum value (~ 2.2 K) at approximately 2.5 GPa from the AFM quantum critical point (QCP), which lies at $P_{QCP}\sim 2.1$ GPa [see Fig. 4(c)].[10] In the region where P exceeds 2.1 GPa, non-Fermi-liquid behaviors, which were probed by the resistivity measurements,[5] were observed and NQR measurements revealed the development of AFM spin fluctuations.[10] $CeTIn_5$, Ce_2TIn_8, and $CeIn_3$ (T=Co, Rh, Ir) are a series of structurally related materials with chemical compositions of the form Ce_mTIn_{3m+2} with $m=1,2,\infty$, respectively. Ce_2TIn_8 enables us to study the relationship between the structure-based evolution of magnetic characteristics and the onset of unconventional SC in HF systems.

Ce_2RhIn_8 is an antiferromagnet with $T_N=2.8$ K at $P=0$.[11] The collinear antiferromagnetic structure with a magnetic wave vector $Q=(1/2,1/2,0)$ and a magnetic moment of $0.55\mu_B$ per Ce ion was reported from the neutron-scattering measurements.[11] The pressure-temperature (P-T) phase diagrams of Ce_2RhIn_8 reported thus far are based on resistivity, ac-susceptibility, and heat-capacity measurements.[12–15] The resistivity measurements revealed that as P increases, T_N monotonously decreases down to 1.2 K at 1.5 GPa; further, SC occurs for $P>1$ GPa and exhibits the maximum T_c ($T_c^{max}\sim 2$ K) around 2.3 GPa. On the other hand, the heat-capacity measurements indicated that an AFM order survives up to $P=1.65$ GPa, but no anomalies that signal the onset of SC were observed. The previously reported NQR-$1/T_1$ measurement was performed to investigate the onset of SC with $T_c=0.9$ K at $P=1.87$ GPa.[16] In this context, a P-T phase diagram for Ce_2RhIn_8 is not yet fully understood.

II. EXPERIMENTAL PROCEDURE

For obtaining NQR measurements, Ce_2RhIn_8 grown by the self-flux method was moderately crushed into a coarse powder to allow RF pulses to easily penetrate the sample. Hydrostatic pressure was applied using a NiCrAl-BeCu piston-cylinder cell filled with a Si-based organic liquid as the pressure-transmitting medium.[17] To calibrate the pressure at low temperatures, the shift in the T_c of Sn metal was monitored by using the resistivity measurements. Figure 1 illustrates the crystal structure of Ce_2RhIn_8, which consists of alternating layers of $CeRhIn_5$ and $CeIn_3$. There are three In sites per unit cell, denoted by In(1), In(2), and In(3). In(1) and In(2) are located in the $CeRhIn_5$ layer, shown in Fig. 1, and In(3) is located in the $CeIn_3$ layer. The measurements for the ^{115}In-NQR ($I=9/2$) spectrum were mainly performed at the $3\nu_Q$ transition at In(2) in Ce_2RhIn_8. Here, ν_Q is defined by the NQR Hamiltonian, $\mathcal{H}_Q=(h\nu_Q/6)[3I_z^2-I(I+1)+\eta(I_x^2-I_y^2)]$, where η is the asymmetry parameter of the electric field gradient. Using $\nu_Q=16.41$ MHz and $\eta=0.43$, the NQR frequency of the $3\nu_Q$ transition is estimated as 47.4 MHz for In(2) at $P=0$. When an internal magnetic field H_{int} is present at the In site during the onset of AFM, the NQR Hamiltonian is perturbed by the Zeeman interaction, which is given by $\mathcal{H}_{AFM}=-\gamma\hbar\vec{I}\cdot\vec{H}_{int}+\mathcal{H}_Q$. A broadening of the NQR spectrum due to H_{int} signals the onset of AFM.

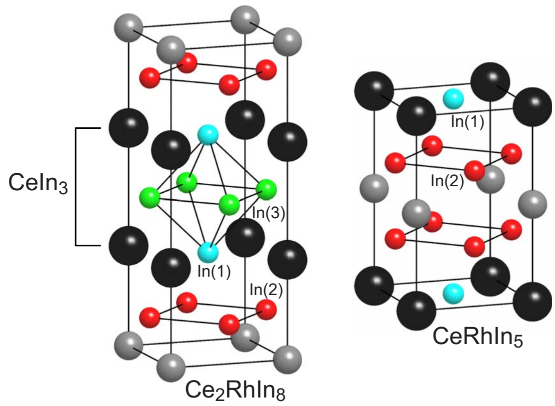

FIG. 1. (Color online) Crystal structures of Ce_2RhIn_8 and $CeRhIn_5$.

III. RESULTS AND DISCUSSION

Figure 2(a) shows the T dependence of $1/T_1$ at high T and $P=0-2.27$ GPa in Ce_2RhIn_8. A distinct peak in $1/T_1$ is associated with the onset of AFM order at $T_N=2.85$ K and $P=0$ GPa. It was reported from the resistivity measurements that the secondary anomaly (T_{LN}) well below T_N was observed in the vicinity of ambient P.[12] However, it was not observed from the present NQR measurements either, as reported in the previous NQR paper by Fukazawa *et al.*[16] Note that in the PM state, $1/T_1$ increases up to 200 K at $P=0$, suggesting that Ce-derived magnetic fluctuations occur in an itinerant regime; this is consistent with the NQR measurement results[16] and the angle-resolved photoemission spectroscopy results.[18] The behavior $1/T_1 \propto T^{1/4}$ is consistent with a quasi-two-dimensional (quasi-2D) AFM spin-fluctuations (SFs) model that predicts the relation $1/T_1T \propto \chi_Q(T)^{3/4}$ near an AFM QCP.[19] Here, the term quasi-2D AFM SFs implies that the magnetic-correlation length in the tetragonal plane develops at a faster rate than that along the c axis and that the staggered susceptibility $\chi_Q(T)$ with the AFM wave vector $Q=(1/2,1/2,0)$ is anticipated to obey the Curie-Weiss law as $\chi_Q(T) \propto 1/(T+\theta)$. In this context, it is predicted that the quasi-2D AFM SFs will obey $1/T_1 \propto T \times \chi_Q(T)^{3/4} \propto T^{1/4}$ in the vicinity of the AFM QCP, where $\theta \sim 0$. As P increases, the T_N determined from a peak in $1/T_1$ decreases to $T_N=1.2$ K at $P=0.92$ GPa. At $P=1.36$ GPa, a marked decrease in $1/T_1$ below 0.9 K without an accompanying peak was observed, which was unexpected. As mentioned later, this is because SC sets in below $T_c=0.9$ K.

Next, we deal with the possible existence of the AFM-QCP in Ce_2RhIn_8. The inset in Fig. 3 shows the $3\nu_Q$-NQR spectra corresponding to In(2) above and below T_N at $P=0$. The main peak inherent to In(2) in Ce_2RhIn_8 is accompanied by two satellite peaks at ~45.8 and ~48.2 MHz, which are thought to be due to stacking faults in the Ce_2RhIn_8 that consists of alternating layers of $CeRhIn_5$ and $CeIn_3$ since the spectral intensities of these peaks are almost negligible. In fact, the x-ray diffraction measurements revealed a diffuse scattering suggesting stacking faults along the c axis of Ce_2RhIn_8.[20] The full width at the half maximum $\sigma(T)$ of the $3\nu_Q$-NQR spectrum increases due to H_{int} induced by the AFM moments that develop below T_N. Figure 3 shows the T dependence of $\Delta\sigma(T)$ at In(2) in Ce_2RhIn_8 for several pressures. Here, $\Delta\sigma(T)=\sigma(T)-\sigma(T_N)$, which is approximately proportional to the magnitude of the AFM ordered moment. At $P=0$, $\Delta\sigma(T)$ is well fitted by the relation $\Delta\sigma(T) \propto [1-(T/T_N)^{3/2}]^{1/2}$, which is expected in a weak itinerant AFM,[21,22] as indicated by the solid line in Fig. 3. Using this relation for $\Delta\sigma(T)$ under P, we tentatively estimate $\Delta\sigma(T=0)$, as shown in Fig. 4(a). Note that as P increases, $\Delta\sigma(T=0)$ decreases linearly and a rough extrapolation to $\Delta\sigma=0$ yields $P_{\mathrm{QCP}} \sim 1.36$ GPa. Furthermore, note that as P increases, the behavior $1/T_1 \propto T^{1/4}$ at $P=0$ evolves into $1/T_1 \propto T^{1/2}$ around P_{QCP}, as shown in Fig. 2(a). The latter relation is consistent with the 3D-AFM SFs model that predicts the relation $1/T_1T \propto \chi_Q(T)^{1/2}$ near the 3D-AFM QCP.[23] When assuming a simple power-law dependence for $1/T_1$, e.g., $1/T_1=AT^n$ with parameters A and n, the systematic T variations in $1/T_1$ are fitted in the T range from T well above T_N(or T_c) to 30 K to obtain the P dependence of n, as shown in Fig. 4(a). Note that n progressively increases up to $n=0.5$ at $P_{\mathrm{QCP}}=1.36$ GPa and remains almost constant as P increases further, indicating that the crossover from the quasi-2D to 3D character of AFM SFs occurs between $P=0$ and 1.36 GPa.

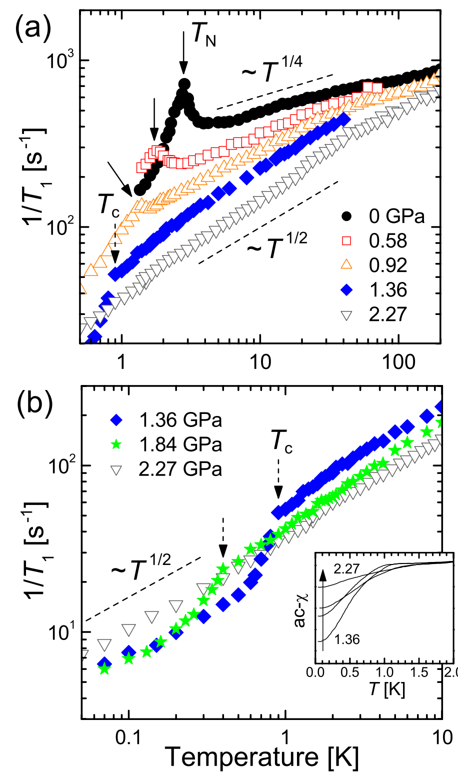

FIG. 2. (Color online) T dependences of $1/T_1$ at (a) high T and (b) at low T for $P=0-2.27$ GPa in Ce_2RhIn_8. Solid and dashed arrows point to T_N and T_c, respectively. The inset shows the T dependence of ac susceptibility at $P=1.36$, 1.62, 1.84, and 2.27 GPa in the order indicated by the direction of the arrow.

Previous papers reported that $1/T_1$ at In(1) differs from that at In(2).[16] We have confirmed that $1/T_1$ at In(3) resembles the corresponding result for In(2), but above $T^* \sim 8$ K, $1/T_1$ at In(1) deviates from the $T^{1/4}$ behavior, as shown in Fig. 5(a). Note that the In-site dependence of $1/T_1$

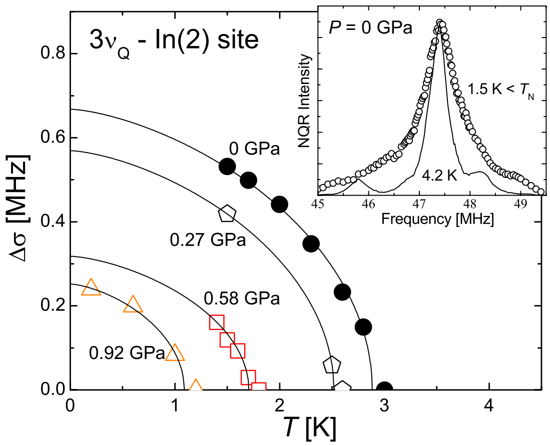

FIG. 3. (Color online) The T dependence of $\Delta\sigma(T)$ at In(2) in Ce_2RhIn_8 for several pressures. The solid lines represent the relation $\Delta\sigma(T)\propto[1-(T/T_N)^{3/2}]^{1/2}$. The inset shows the NQR spectra above and below T_N at $P=0$ GPa.

was also observed in $CeCoIn_5$, as shown in Fig. 5(b). This is understood in terms of the T dependence of the hyperfine-coupling constants at In sites under a crystal electric field (CEF) effect. As a matter of fact, the NMR study reported by Curro *et al.*[24] revealed that the energy splitting between the first excited CEF level and the ground state (Δ_{CEF}) is estimated at 34 K and hence the hyperfine couplings at In(2) significantly changes around 50 K close to $T^*\sim 40$ K. Likewise, since Δ_{CEF} in Ce_2RhIn_8 is estimated at 14 K that was deduced from the magnetic susceptibility and magnetization measurements,[14] the hyperfine couplings at In(1) in this compound may change around a temperature close to $T^*\sim 8$ K.

In order to demonstrate the onset of SC in Ce_2RhIn_8, in Fig. 2(b), we present the T dependences of $1/T_1$ at low T and $P=1.36$, 1.84, and 2.27 GPa, where the AFM order collapses. Although the onset of SC is proved by the appearance of SC diamagnetism, as indicated in the inset in Fig. 2(b), this diamagnetism cannot be used to identify a transition temperature T_c for bulk SC inherent to Ce_2RhIn_8 under P. In fact, the SC diamagnetism for $P>1.84$ GPa starts to appear from a relatively high T onwards. This may be associated with the diamagnetism arising from the $CeRhIn_5$ contained in the sample as an impurity phase. This $CeRhIn_5$ contamination leads to inconsistencies among P-T phase diagrams, depending on the experimental methods.[12–15] On the other hand, a marked reduction in the T dependence of $1/T_1$, which is shown in Fig. 2(b), provides microscopic evidence for the development of SC in the sample at $T_c=0.9$ and 0.4 K and $P=1.36$ and 1.84 GPa, respectively. In contrast, the $1/T_1$ value at 2.27 GPa does not yield such evidence, though the diamagnetism starts to appear below ~ 1.5 K. Thus, material-selective NQR-T_1 measurements allow us to identify the onset of the SC inherent to Ce_2RhIn_8 under P. It is remarkable that significantly large diamagnetism and SC with $T_c^{max}=0.9$ K are observed at $P_{QCP}=1.36$ GPa. These results suggest the intimate relationship between the unconventional SC and the AFM QCP in Ce_2RhIn_8. Furthermore, it should be noted that SC sets in as a result of the evolution from the quasi-2D to 3D character of AFM SFs. This is in

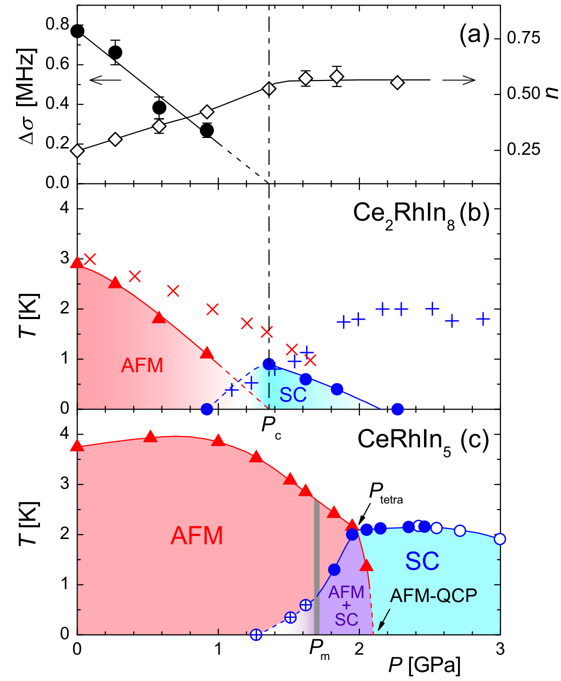

FIG. 4. (Color online) (a) The P dependence of $\Delta\sigma(T=0)$ at In(2) and n where $1/T_1\propto T^n$ in the PM state at temperatures well above T_N (or T_c). (b) The P-T phase diagram of Ce_2RhIn_8. The data denoted by cross and plus marks indicate the P dependences of T_N and T_c, as determined from heat-capacity (Ref. 15) and resistivity (Ref. 12) measurements, respectively. (c) The P-T phase diagram of $CeRhIn_5$ (Refs. 10 and 28). The commensurate AFM is completely realized above P_m.

contrast to the fact that the SC dome in $CeCoIn_5$ and $CeRhIn_5$ with $T_c^{max}>2$ K is realized around the quasi-2D AFM QCP but is separated from the phase boundary between the AFM and PM phases. These results demonstrate the intimate relationship between the dimensionality of AFM SFs and the onset of unconventional SC; the 2D character of AFM SFs is favorable to the increase in the T_c in HF SC compounds as well as in high-T_c copper oxides.[25]

As an indication that the symmetry of the SC gap function in Ce_2RhIn_8 must be considered, we note that $1/T_1$ at $P=1.36$ GPa decreases without the appearance of a coherence peak just below T_c and exhibits a large kink well below T_c, associated with the existence of the large residual density of states. These results suggest a dirty d-wave SC with line-nodes gap, identical to the case of high-T_c superconductors.[26] This may be because difficulties in preparing the crystals containing alternating layers of $CeRhIn_5$ and $CeIn_3$ lead to impurities and/or crystal imperfections like stacking faults in Ce_2RhIn_8. It is well known that the existence of the residual density of states due to the impurity effect results in T-linear behavior well below T_c. Unexpectedly, however, the observed behavior $1/T_1\propto T^{1/2}$ well below T_c cannot be simply explained by the impurity effect for unconventional SC; this indicates the persistence of low-lying excitations in the SC state due to the proximity to the AFM QCP. The enhancement of $1/T_1$ even at temperatures lower than T_c is also observed in the uniformly coexisting state of SC and AFM around the AFM-QCP in $CeCu_2Si_2$,[27] $CeRhIn_5$,[28]

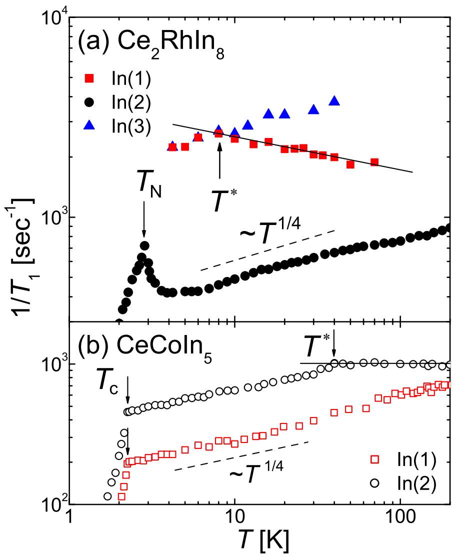

FIG. 5. (Color online) (a) The T dependence of $1/T_1$ for the In(1), In(2), and In(3) sites at ambient P in Ce_2RhIn_8. (b) The T dependence of $1/T_1$ for the In(1) (Ref. 33) and In(2) sites at ambient P in $CeCoIn_5$. The solid lines are eyes guides. T^* is the temperature at which the anomaly in the T dependence of $1/T_1$ appears.

$CeCo(In_{1-x}Cd_x)_5$,[29] and $CeNiGe_3$.[30] However, note that in Ce_2RhIn_8, the behavior of $1/T_1 \propto T^{1/2}$ is observed even in the SC state where the AFM order collapses. In this context, the P-T phase diagram for Ce_2RhIn_8 is the only one that reveals the following unconventional SC characteristic: 3D-AFM SFs survive in the SC state that occurs in the relatively narrow P range 1.36–1.84 GPa.

IV. CONCLUSION

In conclusion, we have established the P-T phase diagram for Ce_2RhIn_8 from microscopic In-NQR measurements. The AFM order disappears at $P_{QCP}\sim 1.36$ GPa, where 3D-AFM SFs are dominant. It was demonstrated that the SC order occurs in the narrow P range of 1.36–1.84 GPa and exhibits $T_c^{max}=0.9$ K around $P_{QCP}\sim 1.36$ GPa. We state that this phase diagram differs from the previously reported ones[12,15] because the latter were affected by contamination by impurity phases such as $CeRhIn_5$. The unconventional SC in Ce_2RhIn_8 occurs under the development of 3D AFM SFs rather than the quasi-2D AFM SFs, as in the case of $CeCoIn_5$ (Refs. 31–33) and $CeRhIn_5$.[5] Noting that the T_c^{max} (=0.9 K) for Ce_2RhIn_8 is significantly lower than the T_c(>2 K) for $CeCoIn_5$ and $CeRhIn_5$, it is suggested that the 2D character of AFM SFs plays a vital role in increasing the T_c in strongly correlated electron systems.

ACKNOWLEDGMENTS

This work was supported by Grants-in-Aid for Specially Promoted Research (Grant No. 20001004) and for Young Scientists (B) (Grant No. 20740195) from the Ministry of Education, Culture, Sports, Science and Technology (MEXT) of Japan. It was partially supported by the Global COE Program (Core Research and Engineering of Advanced Materials-Interdisciplinary Education Center for Materials Science) from MEXT.

*Present address: Department of Physics, Kyoto University, Kyoto 606-8502, Japan.

[1] N. D. Mathur, F. M. Grosche, S. R. Julian, I. R. Walker, D. M. Freye, R. K. W. Haselwimmer, and G. G. Lonzarich, Nature (London) **394**, 39 (1998).

[2] G. Knebel, D. Braithwaite, P. C. Canfield, G. Lapertot, and J. Flouquet, Phys. Rev. B **65**, 024425 (2001).

[3] C. Petrovic, P. G. Pagliuso, M. F. Hundley, R. Movshovich, J. L. Sarrao, J. D. Thompson, Z. Fisk, and P. Monthoux, J. Phys.: Condens. Matter **13**, L337 (2001).

[4] H. Hegger, C. Petrovic, E. G. Moshopoulou, M. F. Hundley, J. L. Sarrao, Z. Fisk, and J. D. Thompson, Phys. Rev. Lett. **84**, 4986 (2000).

[5] T. Muramatsu, N. Tateiwa, T. C. Kobayashi, K. Shimizu, K. Amaya, D. Aoki, H. Shishido, Y. Haga, and Y. Ōnuki, J. Phys. Soc. Jpn. **70**, 3362 (2001).

[6] C. Petrovic, R. Movshovich, M. Jaime, P. G. Pagliuso, M. F. Hundley, J. L. Sarrao, Z. Fisk, and J. D. Thompson, Europhys. Lett. **53**, 354 (2001).

[7] Y. Kitaoka, S. Kawasaki, T. Mito, and Y. Kawasaki, J. Phys. Soc. Jpn. **74**, 186 (2005).

[8] S. Kawasaki, T. Mito, Y. Kawasaki, H. Kotegawa, G.-q. Zheng, Y. Kitaoka, H. Shishido, S. Araki, R. Settai, and Y. Ōnuki, J. Phys. Soc. Jpn. **73**, 1647 (2004).

[9] S. Kawasaki, M. Yashima, Y. Kitaoka, K. Takeda, K. Shimizu, Y. Oishi, M. Takata, T. C. Kobayashi, H. Harima, S. Araki, H. Shishido, R. Settai, and Y. Ōnuki, Phys. Rev. B **77**, 064508 (2008).

[10] M. Yashima, S. Kawasaki, H. Mukuda, Y. Kitaoka, H. Shishido, R. Settai, and Y. Ōnuki, Phys. Rev. B **76**, 020509(R) (2007).

[11] W. Bao, P. G. Pagliuso, J. L. Sarrao, J. D. Thompson, Z. Fisk, and J. W. Lynn, Phys. Rev. B **64**, 020401(R) (2001).

[12] M. Nicklas, V. A. Sidorov, H. A. Borges, P. G. Pagliuso, C. Petrovic, Z. Fisk, J. L. Sarrao, and J. D. Thompson, Phys. Rev. B **67**, 020506(R) (2003).

[13] S. Ohara, Y. Shomi, and I. Sakamoto, Physica B (Amsterdam) **329–333**, 612 (2003).

[14] T. Ueda, H. Shishido, S. Hashimoto, T. Okubo, M. Yamada, Y. Inada, R. Settai, H. Harima, A. Galatanu, E. Yamamoto, N. Nakamura, K. Sugiyama, T. Takeuchi, K. Kindo, T. Namiki, Y. Aoki, H. Sato, and Y. Ōnuki, J. Phys. Soc. Jpn. **73**, 649 (2004).

[15] E. Lengyel, J. L. Sarrao, G. Sparn, F. Steglich, and J. D. Thompson, J. Magn. Magn. Mater. **272–276**, 52 (2004).

[16] H. Fukazawa, T. Okazaki, K. Hirayama, Y. Kohori, G. Chen, S. Ohara, I. Sakamoto, and T. Matsumoto, J. Phys. Soc. Jpn. **76**, 124703 (2007).

[17] A. S. Kirichenko, A. V. Kornilov, and V. M. Pudalov, Instrum. Exp. Tech. **48**, 813 (2005).

[18] S. Raj, Y. Iida, S. Souma, T. Sato, T. Takahashi, H. Ding, S. Ohara, T. Hayakawa, G. F. Chen, I. Sakamoto, and H. Harima, Phys. Rev. B **71**, 224516 (2005).
[19] C. Lacroix, A. Solontsov, and R. Ballou, Phys. Rev. B **54**, 15178 (1996).
[20] M. Koeda, T. Fujiwara, M. Hedo, Y. Uwatoko, H. Sagayama, Y. Wakabayashi, and H. Sawa, J. Magn. Magn. Mater. **310**, e31 (2007).
[21] K. Nakayama and T. Moriya, J. Phys. Soc. Jpn. **56**, 2918 (1987).
[22] H. Hasegawa and T. Moriya, J. Phys. Soc. Jpn. **36**, 1542 (1974).
[23] T. Moriya and K. Ueda, Solid State Commun. **15**, 169 (1974).
[24] N. J. Curro, B. Simovic, P. C. Hammel, P. G. Pagliuso, J. L. Sarrao, J. D. Thompson, and G. B. Martins, Phys. Rev. B **64**, 180514(R) (2001).
[25] B. A. Scott, E. Y. Suard, C. C. Tsuei, D. B. Mitzi, T. R. McGuire, B.-H. Chen, and D. Walker, Physica C **230**, 239 (1994).
[26] K. Ishida, Y. Kitaoka, N. Ogata, T. Kamino, K. Asayama, J. R. Cooper, and N. Athanassopoulou, J. Phys. Soc. Jpn. **62**, 2803 (1993).
[27] Y. Kawasaki, K. Ishida, K. Obinata, K. Tabuchi, K. Kashima, Y. Kitaoka, O. Trovarelli, C. Geibel, and F. Steglich, Phys. Rev. B **66**, 224502 (2002).
[28] M. Yashima, H. Mukuda, Y. Kitaoka, H. Shishido, R. Settai, and Y. Ōnuki, Phys. Rev. B **79**, 214528 (2009).
[29] R. R. Urbano, B.-L. Young, N. J. Curro, J. D. Thompson, L. D. Pham, and Z. Fisk, Phys. Rev. Lett. **99**, 146402 (2007).
[30] A. Harada, H. Mukuda, Y. Kitaoka, A. Thamizhavel, Y. Okuda, R. Settai, Y. Ōnuki, K. M. Itoh, E. E. Haller, and H. Harima, J. Phys. Soc. Jpn. **77**, 103710 (2008).
[31] V. A. Sidorov, M. Nicklas, P. G. Pagliuso, J. L. Sarrao, Y. Bang, A. V. Balatsky, and J. D. Thompson, Phys. Rev. Lett. **89**, 157004 (2002).
[32] Y. Kawasaki, S. Kawasaki, M. Yashima, T. Mito, G.-q. Zheng, Y. Kitaoka, H. Shishido, R. Settai, Y. Haga, and Y. Ōnuki, J. Phys. Soc. Jpn. **72**, 2308 (2003).
[33] M. Yashima, S. Kawasaki, Y. Kawasaki, G.-q. Zheng, Y. Kitaoka, H. Shishido, R. Settai, Y. Haga, and Y. Ōnuki, J. Phys. Soc. Jpn. **73**, 2073 (2004).